OPEN ACCESS

International
Journal
Of Modern Engineering Research (IJMER)

Robust Sliding Mode Control Design for DC Motor Drives under Load Disturbances and Parameter Uncertainties

Do Quy Quan[1], Nguyen Trung Thanh[2], Tran Minh Hai[3*]
[1]*Faculty of Electrical and Electronic, Hung Yen College*
[2]*Thai Nguyen University of Technology*
[3]*Faculty of Technology and Engineering, Thai Binh University*

Abstract
This paper presents the design of a Sliding Mode Control (SMC) scheme for speed regulation of a DC motor subject to load-torque disturbances and parameter variations, with a conventional PID controller employed as a benchmark for comparison. The objective is to evaluate the speed-tracking performance, closed-loop stability, and robustness of the two control strategies under different operating conditions.
An electromechanical model of the DC motor is established and used as a common basis for the design of both controllers. For the SMC scheme, the control law is formulated in terms of the speed-tracking error, and closed-loop stability is analyzed using Lyapunov theory. A saturation function is further introduced to mitigate chattering and to improve compatibility with the physical constraints of the actuator.
The two control strategies are evaluated under nominal operating conditions, load disturbances, and motor parameter variations. Simulation results show that PID provides a faster transient response under nominal conditions, whereas SMC maintains smaller tracking errors and exhibits superior disturbance-rejection capability as the operating conditions vary. These results indicate that SMC is a promising solution for DC motor drive systems requiring reliable speed tracking, enhanced disturbance rejection, and sustained control performance in the presence of model uncertainties.

Index Terms*: DC motor, sliding mode control (SMC), PID control, speed control, load disturbance, robust control, Lyapunov stability.*

Date of Submission: 12-09-2026 Date of acceptance: 23-09-2026

I. INTRODUCTION

Direct-current (DC) motors remain widely used in a variety of electric drive systems owing to their relatively simple structure, favorable torque characteristics, and wide speed-regulation range [1], [2]. In applications such as robotics, actuators, automated systems, and precision drives, speed-control performance directly affects the accuracy and overall performance of the system. In practical operation, however, DC motor drives are commonly subjected to load-torque disturbances and variations in parameters such as armature resistance, rotor inertia, and viscous friction, which may degrade tracking performance and closed-loop dynamic behavior [1], [3], [4].

Proportional–integral–derivative (PID) control remains one of the most widely adopted approaches for DC motor speed regulation because of its simple structure, intuitive tuning procedure, and ease of practical implementation [2], [5]. Under operating conditions close to the nominal point, a properly tuned PID controller can provide satisfactory transient performance and a small steady-state error. Nevertheless, its performance is closely related to controller tuning and the dynamic characteristics of the plant. Variations in load torque and motor parameters may therefore lead to degraded tracking and disturbance-recovery performance [4]–[6]. This limitation motivates the investigation of control strategies capable of maintaining satisfactory performance in the presence of disturbances and model uncertainties.

Sliding Mode Control (SMC) is a nonlinear control methodology that has been extensively investigated because of its robustness against certain classes of external disturbances and parametric uncertainties [7]–[10]. The fundamental principle of SMC is to define an appropriate sliding manifold and construct a control law that drives the system trajectories toward this manifold and subsequently maintains the system motion on, or within a neighborhood of, the sliding surface [7], [8]. Once the sliding regime is established, the closed-loop dynamics can exhibit reduced sensitivity to bounded uncertainties and disturbances [9], [10]. However, the discontinuous switching action inherent in conventional SMC may induce high-frequency oscillations known as chattering, which can degrade control quality and limit practical implementation [9], [11]. Boundary-layer approximations and higher-order sliding-mode techniques have therefore been widely investigated to alleviate this phenomenon [10], [11].

The robustness properties of sliding-mode-based approaches have motivated their application to electromechanical and motor-drive systems [10], [12]. For DC motor control in particular, previous studies have demonstrated that sliding-mode strategies can provide effective tracking performance in the presence of parameter uncertainties and external disturbances [12]–[14]. Experimental and simulation studies have also reported favorable disturbance-rejection characteristics of SMC compared with conventional linear controllers, although the resulting performance strongly depends on the controller structure, switching gain, actuator constraints, and chattering-mitigation strategy [12]–[14].

Motivated by these considerations, this study develops an SMC scheme for speed regulation of a DC motor subject to load-torque disturbances and parameter variations, while a conventional PID controller is employed as a benchmark. An electromechanical model of the motor is established and consistently used for the design and evaluation of both controllers. For the SMC scheme, the sliding surface is constructed from the speed-tracking error, and the control law is formulated using equivalent and switching control components. Closed-loop stability is analyzed within a Lyapunov framework, while a saturation function is employed to mitigate chattering and accommodate the physical limitation of the control input.

The study focuses on three main aspects: the design of an SMC scheme for DC motor speed tracking together with analysis of its convergence condition; evaluation of disturbance-rejection capability and robustness under variations in load torque and motor parameters; and direct comparison with PID control under identical simulation conditions. Transient-response characteristics and integral error indices are employed to quantify the differences between the two approaches under nominal operation and in the presence of disturbances.

The remainder of this paper is organized as follows. Section 2 presents the mathematical model of the DC motor together with the disturbance and uncertainty descriptions. Section 3 describes the design of the PID and SMC controllers and provides the corresponding stability analysis. Section 4 presents the simulation setup, comparative results, and discussion. Finally, Section 5 summarizes the main conclusions of the study.

II. SYSTEM MODEL AND THEORETICAL BACKGROUND

2.1. Mathematical Model of the DC Motor

According to Kirchhoff's voltage law, the armature-circuit dynamics of the DC motor are described by the following electrical equation [1], [2]:

$$L_a \frac{di_a(t)}{dt} = -R_a i_a(t) - K_e \omega(t) + u(t) \tag{1}$$

where R_a and L_a denote the armature resistance and inductance, respectively; $i_a(t)$ is the armature current; and K_e is the back-electromotive-force constant.

The electromagnetic torque generated by the motor is proportional to the armature current:

$$T_e(t) = K_t i_a(t) \tag{2}$$

where K_t is the torque constant.

The rotor mechanical dynamics are obtained from the torque-balance equation:

$$J \frac{d\omega(t)}{dt} = T_e(t) - B\omega(t) - T_L(t) \tag{3}$$

where J is the equivalent rotor inertia, B is the viscous friction coefficient, and $T_L(t)$ is the load torque applied to the shaft.

Substituting (2) into (3) yields

$$J \frac{d\omega(t)}{dt} = K_t i_a(t) - B\omega(t) - T_L(t) \tag{4}$$

From (1) and (4), the DC motor dynamics can be written as

$$i_a(t) = -\frac{R_a}{L_a} i_a(t) - \frac{K_e}{L_a}\omega(t) + \frac{1}{L_a}u(t) \tag{5}$$

and

$$\dot{\omega}(t) = \frac{K_t}{J} i_a(t) - \frac{B}{J}\omega(t) - \frac{1}{J}T_L(t) \tag{6}$$

Define the state vector as

$$\mathbf{x}(t) = \begin{bmatrix} i_a(t) \\ \omega(t) \end{bmatrix} \tag{7}$$

Then, (5)–(6) can be expressed in state-space form as

$$\dot{\mathbf{x}}(t) = \mathbf{A}\mathbf{x}(t) + \mathbf{B}_u u(t) + \mathbf{B}_d T_L(t) \tag{8}$$

where

$$\mathbf{A} = \begin{bmatrix} -\frac{R_a}{L_a} & -\frac{K_e}{L_a} \\ \frac{K_t}{J} & -\frac{B}{J} \end{bmatrix}, \quad \mathbf{B}_u = \begin{bmatrix} \frac{1}{L_a} \\ 0 \end{bmatrix}, \quad \mathbf{B}_d = \begin{bmatrix} 0 \\ -\frac{1}{J} \end{bmatrix} \tag{9}$$

The controlled output is the rotor speed:

$$y(t) = \omega(t) = [0 \quad 1]\mathbf{x}(t) \tag{10}$$

It follows from (5)–(6) that the control voltage $u(t)$ acts directly on the armature-current dynamics but does not appear explicitly in the first derivative of the rotor speed. Consequently, for armature-voltage speed control, the control input enters the system when the second derivative of the rotor speed is considered. This relative-degree property motivates the sliding-surface structure adopted in the SMC design.

2.2. Disturbance, Uncertainty, and Control Problem Formulation

In practical DC motor drives, speed-control performance is affected not only by the nominal plant dynamics but also by load variations and parameter uncertainties [4], [12], [13]. In this study, the load torque is treated as the principal external disturbance acting on the system.

The load torque is represented in the general form

$$T_L(t) = T_{L0} + \Delta T_L(t) \tag{11}$$

where T_{L0} denotes the nominal load component and $\Delta T_L(t)$ represents the time-varying load disturbance.

To evaluate disturbance-rejection performance, a sudden load variation is modeled as

$$\Delta T_L(t) = T_d H(t - t_d) \tag{12}$$

where T_d is the load-torque increment, t_d is the disturbance application time, and $H(\cdot)$ denotes the unit-step function.

Model (12) is employed in the simulations to impose a clear and repeatable load variation on both closed-loop systems. In a physical drive, the load transition occurs over a finite interval; therefore, the actual disturbance and its rate of variation can reasonably be assumed to be bounded.

In addition to load disturbances, motor parameters may vary because of temperature changes, load reconfiguration, or identification errors. A generic uncertain parameter p is represented as

$$p = p_0(1 + \delta_p), \qquad |\delta_p| \le \bar{\delta}_p \tag{13}$$

where p_0 is the nominal value, δ_p denotes the relative parameter variation, and $\bar{\delta}_p$ is the corresponding uncertainty bound.

In this study, variations in the armature resistance R_a, rotor inertia J, and viscous friction coefficient B are considered. Variations in R_a account for temperature-dependent changes in the armature winding, whereas variations in J and B represent changes in the mechanical loading characteristics.

The following assumptions are introduced for controller design and stability analysis.

Assumption 1: The reference speed $\omega_{\text{ref}}(t)$ is bounded and differentiable to the order required by the control law. The signals $\dot{\omega}_{\text{ref}}(t)$ and $\ddot{\omega}_{\text{ref}}(t)$ exist and are bounded.

Assumption 2: The physical load torque and its rate of variation are bounded; that is, there exist positive constants $\bar{T}_L$ and $\bar{d}_L$ such that

$$|T_L(t)| \le \bar{T}_L, \qquad |\dot{T}_L(t)| \le \bar{d}_L \tag{14}$$

Assumption 3: The physical motor parameters are positive and remain within known bounded intervals:

$$0 < p_{\min} \le p(t) \le p_{\max} \tag{15}$$

Assumption 4: The armature voltage is limited by the power converter according to

$$|u(t)| \le U_{\max} \tag{16}$$

Assumption (16) is important for the comparative evaluation because a theoretically computed control input may exceed the voltage capability of the actuator. Applying the same limit $U_{\max}$ to PID and SMC ensures that both controllers are evaluated under identical physical constraints.

The speed-tracking error is defined as

$$e(t) = \omega(t) - \omega_{\text{ref}}(t) \tag{17}$$

Under ideal conditions, the control law $u(t)$ is required to guarantee closed-loop stability and

$$\lim_{t\to\infty} e(t) = 0 \tag{18}$$

When actuator limits, disturbances, parameter uncertainties, and the SMC boundary layer are taken into account, the practical objective is relaxed to maintaining the tracking error within a sufficiently small neighborhood:

$$|e(t)| \le \varepsilon_e, \qquad t \ge t_s \tag{19}$$

where $\varepsilon_e > 0$ denotes the admissible tracking-error bound.

For quantitative assessment of tracking and disturbance-rejection performance, the root-mean-square (RMS) error, integral absolute error (IAE), integral time-weighted absolute error (ITAE), and overshoot are considered in addition to standard transient-response measures [2], [3].
The RMS tracking error is defined as

$$e_{\mathrm{RMS}} = \sqrt{\frac{1}{T}\int_{t_0}^{t_0+T} e^2\,(t)\,dt} \tag{20}$$

The RMS metric quantifies the effective magnitude of the tracking error over the evaluation interval; a smaller RMS value indicates that the motor speed remains closer to the reference.
The IAE is defined as

$$IAE = \int_{t_0}^{t_0+T} |e(t)|\,dt \tag{21}$$

whereas the ITAE is given by

$$ITAE = \int_{t_0}^{t_0+T} (t - t_0)\,|e(t)|\,dt \tag{22}$$

The IAE measures the accumulated absolute tracking error, whereas the ITAE imposes a larger penalty on errors that persist for longer periods. Accordingly, the ITAE is particularly useful for characterizing post-disturbance recovery.
The percentage overshoot is defined as

$$M_p = \frac{\omega_{\max} - \omega_{\mathrm{ref}}}{\omega_{\mathrm{ref}}} \times 100\% \tag{23}$$

The indices in (20)–(23) are used consistently in the PID–SMC comparison to assess nominal speed tracking as well as the preservation of control performance under load disturbances and parameter variations.

III. CONTROLLER DESIGN

3.1. PID Controller

A conventional PID controller is employed as the benchmark for evaluating the proposed SMC strategy. PID control is widely used in motor-drive applications because of its simple structure and practical tuning characteristics [2], [5], [6]. Using the speed-tracking error defined in Section 2, the PID control input is expressed as

$$u_{\mathrm{PID}}(t) = -K_p e(t) - K_i \int_0^t e\,(\tau)\,d\tau - K_d \dot{e}(t) \tag{24}$$

where K_p, K_i, and K_d denote the proportional, integral, and derivative gains, respectively.

The negative sign follows from the error definition $e(t) = \omega(t) - \omega_{\mathrm{ref}}(t)$. When the actual speed exceeds the reference, $e(t) > 0$, the controller reduces the armature voltage; conversely, when the actual speed is below the reference, $e(t) < 0$, the control action is increased to restore the desired speed.
To account for the physical limitation of the power converter, the control signal is constrained as

$$u_{\mathrm{PID}}(t) = \mathrm{sat}_{U_{\max}}\big(u^*_{\mathrm{PID}}(t)\big) \tag{25}$$

with

$$\mathrm{sat}_{U_{\max}}(u) = \begin{cases} U_{\max}, & u > U_{\max}, \\ u, & |u| \le U_{\max}, \\ -U_{\max}, & u < -U_{\max}. \end{cases} \tag{26}$$

In the simulation implementation, an anti-windup mechanism is included to prevent excessive accumulation of the integral term during actuator saturation. The PID gains are tuned under nominal conditions and kept fixed for all subsequent test scenarios.

3.2. Sliding Mode Controller Design

From the mechanical dynamics of the DC motor,

$$\dot{\omega} = \frac{K_t}{J} i_a - \frac{B}{J}\omega - \frac{1}{J} T_L \tag{27}$$

The control input $u(t)$ does not appear explicitly in $\dot{\omega}$. Therefore, if a simple surface of the form $s = e$ is selected, the control input is absent from the first derivative of the sliding variable. Following the classical sliding-mode framework [7]–[10] and accounting for the relative degree from armature voltage to rotor speed, the sliding surface is selected as

$$s(t) = \dot{e}(t) + \lambda e(t), \qquad \lambda > 0 \tag{28}$$

When the sliding regime is established, $s(t) = 0$, and therefore

$$\dot{e}(t) + \lambda e(t) = 0 \tag{29}$$

The resulting tracking-error dynamics on the sliding manifold have the solution

$$e(t) = e(t_s) e^{-\lambda(t - t_s)}, \qquad t \ge t_s \tag{30}$$

where t_s denotes the time at which the trajectory reaches the sliding manifold. Since $\lambda > 0$,

$$\lim_{t\to\infty} e(t) = 0 \tag{31}$$

Hence, once the system trajectory reaches and remains on the sliding manifold, the rotor speed asymptotically converges to the reference value.

3.2.1 Control Law Derivation

Differentiating the sliding variable gives

$$\dot{s} = \ddot{e} + \lambda\dot{e} \tag{32}$$

Since $e = \omega - \omega_{\mathrm{ref}}$, it follows that

$$\dot{e} = \dot{\omega} - \dot{\omega}_{\mathrm{ref}} \tag{33}$$

and

$$\ddot{e} = \ddot{\omega} - \ddot{\omega}_{\mathrm{ref}} \tag{34}$$

Differentiating the mechanical equation yields

$$\ddot{\omega} = \frac{K_t}{J} i_a - \frac{B}{J}\dot{\omega} - \frac{1}{J}\dot{T}_L \tag{35}$$

From the armature electrical dynamics,

$$i_a = -\frac{R_a}{L_a} i_a - \frac{K_e}{L_a}\omega + \frac{1}{L_a}u \tag{36}$$

Substituting the electrical dynamics into the preceding equation gives

$$\ddot{\omega} = -\frac{K_t R_a}{J L_a} i_a - \frac{K_t K_e}{J L_a}\omega + \frac{K_t}{J L_a}u - \frac{B}{J}\dot{\omega} - \frac{1}{J}\dot{T}_L \tag{37}$$

Hence, the sliding-variable dynamics can be expressed as

$$\begin{aligned}\dot{s} = \quad & -\frac{K_t R_a}{J L_a} i_a - \frac{K_t K_e}{J L_a}\omega + \frac{K_t}{J L_a}u \\ & + \left(\lambda - \frac{B}{J}\right)\dot{\omega} - \lambda\dot{\omega}_{\mathrm{ref}} - \ddot{\omega}_{\mathrm{ref}} - \frac{1}{J}\dot{T}_L.\end{aligned} \tag{38}$$

The SMC law is decomposed into two components [7], [9], [10]:

$$u(t) = u_{\mathrm{eq}}(t) + u_{\mathrm{sw}}(t) \tag{39}$$

where u_{eq} is the equivalent-control component and u_{sw} is the switching-control component.
Neglecting the disturbance-rate term in the nominal model and imposing $\dot{s} = 0$ yields the equivalent control

$$u_{\mathrm{eq}} = R_a i_a + K_e\omega - \frac{J L_a}{K_t}\left[\left(\lambda - \frac{B}{J}\right)\dot{\omega} - \lambda\dot{\omega}_{\mathrm{ref}} - \ddot{\omega}_{\mathrm{ref}}\right] \tag{40}$$

For a constant speed reference,

$$\dot{\omega}_{\mathrm{ref}} = \ddot{\omega}_{\mathrm{ref}} = 0$$

and the equivalent control reduces to

$$u_{\mathrm{eq}} = R_a i_a + K_e\omega - \frac{J L_a}{K_t}\left(\lambda - \frac{B}{J}\right)\dot{\omega} \tag{41}$$

The switching component is selected according to the reaching law

$$u_{\mathrm{sw}} = -\frac{J L_a}{K_t} K\operatorname{sign}(s), \qquad K > 0 \tag{42}$$

Accordingly, the ideal SMC law is given by

$$u = u_{\mathrm{eq}} - \frac{J L_a}{K_t} K\operatorname{sign}(s) \tag{43}$$

3.2.2. Stability Analysis of the SMC Scheme

Theorem 1: Consider the DC motor system with the proposed sliding surface and ideal SMC law. If the disturbance satisfies

$$\left|\dot{T}_L(t)\right| \le \bar{d}_L \tag{44}$$

and the switching gain is selected such that

$$K > \frac{\bar{d}_L}{J} \tag{45}$$

then the system trajectory reaches the sliding manifold $s = 0$ in finite time.
Proof: Following the standard Lyapunov stability framework for sliding-mode systems [7], [9], consider the Lyapunov candidate

$$V(s) = \frac{1}{2}s^2 \tag{46}$$

For $s \neq 0$, $V(s) > 0$. The time derivative of the Lyapunov function is

$$\dot{V} = s\dot{s} \tag{47}$$

Substituting the SMC law into the sliding-variable dynamics cancels the nominal terms and yields

$$\dot{s} = -K\operatorname{sign}(s) - \frac{1}{J}\dot{T}_L \tag{48}$$

Therefore,

$$\dot{V} = -K|s| - \frac{1}{J}s\dot{T}_L \tag{49}$$

Using the bounded-disturbance assumption,

$$\left|\frac{1}{J}s\dot{T}_L\right| \le \frac{\bar{d}_L}{J}|s| \tag{50}$$

which gives

$$\dot{V} \le -\left(K - \frac{\bar{d}_L}{J}\right)|s| \tag{51}$$

If $K > \bar{d}_L/J$, then

$$\dot{V} < 0, \qquad s \neq 0 \tag{52}$$

Hence, the state trajectory converges to the sliding manifold $s = 0$. Once the sliding regime is established, the sliding-surface dynamics $\dot{e} + \lambda e = 0$ together with $\lambda > 0$ imply that the tracking error converges to zero:

$$\lim_{t\to\infty} e(t) = 0 \tag{53}$$

This establishes convergence of the closed-loop system under the proposed ideal SMC law.

3.3.3 Chattering Mitigation and Control-Input Constraint

The switching law employs the sign function $\mathrm{sign}(s)$, which is discontinuous at $s = 0$. In practical systems, high-frequency switching may produce chattering, resulting in control-signal oscillations, increased losses, and excitation of unmodeled dynamics [9]–[11].

To alleviate chattering, the sign function is replaced by a continuous saturation function within a boundary layer [9]–[11]:

$$\mathrm{sat}\left(\frac{s}{\phi}\right) = \begin{cases} 1, & s > \phi, \\ \frac{s}{\phi}, & |s| \le \phi, \\ -1, & s < -\phi. \end{cases} \tag{54}$$

where $\phi > 0$ denotes the boundary-layer thickness. The SMC law implemented in the simulations is then expressed as

$$u = u_{\mathrm{eq}} - \frac{JL_a}{K_t} K \mathrm{sat}\left(\frac{s}{\phi}\right) \tag{55}$$

Compared with the sign function, the saturation function reduces the rate of control variation in the vicinity of the sliding manifold. The ideal condition $s = 0$ is consequently replaced by motion within the boundary layer

$$|s| \le \phi \tag{56}$$

Thus, ϕ represents a tradeoff between tracking accuracy and chattering attenuation. As with the PID controller, the SMC input is subject to the physical voltage limit of the converter:

$$u_{\mathrm{SMC}} = \mathrm{sat}_{U_{\max}}(u_{\mathrm{eq}} + u_{\mathrm{sw}}) \tag{57}$$

This constraint is particularly important in practical drive systems because an excessively large switching gain K may cause the control input to reach the actuator limit $U_{\max}$ frequently. In this case, further increasing K no longer produces a proportional increase in effective control authority and instead primarily increases the duration of actuator saturation.

In this study, K is selected according to three criteria: satisfaction of the convergence condition, reduction of the reaching time, and avoidance of excessive voltage saturation. The final values of λ, K, and ϕ are reported in the simulation setup.

IV. SIMULATION RESULTS AND DISCUSSION

4.1. Simulation Setup

The PID and SMC controllers are evaluated using the same DC motor model, reference signal, initial conditions, and voltage constraint to ensure a consistent comparison. The nominal motor parameters are selected as follows:

$$R_a = 2\,\Omega, L_a = 0.5\,\mathrm{H}, K_t = 0.1\,\mathrm{N}\,\frac{\mathrm{m}}{\mathrm{A}}, K_e = 0.1\,\mathrm{V\,s/rad}, J = 0.02\,\mathrm{kg\,m^2}, B = 0.002\,\mathrm{N\,m\,s/rad}.$$

The reference speed is set to $\omega_{\mathrm{ref}} = 80\,\mathrm{rad/s}$, corresponding to approximately $763.94\,\mathrm{rpm.Đ}$. The control voltage is constrained to $|u(t)| \le 24\,\mathrm{V}$..

The PID controller gains are selected as $K_p = 3.7, K_i = 6.4, K_d = 0.55$.

The SMC parameters are selected as $\lambda = 10, K = 220,\ \phi = 3$.

To evaluate disturbance rejection, a step load torque of $T_L = 0.15\,\mathrm{N\,m}$ is applied at $t = 6\,\mathrm{s.}$, after both closed-loop systems have reached a near-steady operating condition. Robustness against model uncertainty is evaluated by varying the motor parameters according to $R'_a = 1.3R_a, J' = 1.5J, B' = 1.4B$, while all controller parameters are kept unchanged.

4.2. Results and Discussion

Under nominal conditions, both PID and SMC track the reference speed with an approximately zero steady-state error. The PID controller exhibits a faster transient response, with a rise time of 1.4196 s and a settling time of 1.9841 s, whereas the corresponding values for SMC are 2.9100 s and 3.6693 s. However, the PID response exhibits an overshoot of approximately 1.3732%, while the SMC response shows essentially no overshoot.

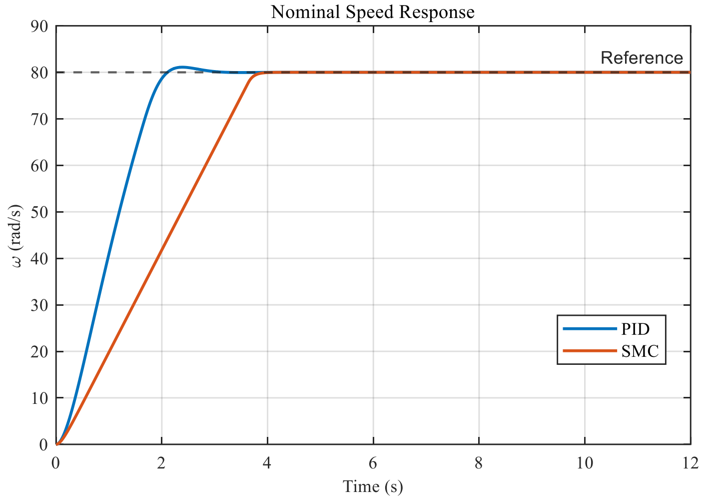

Fig. 1. Speed responses of the DC motor with PID and SMC under nominal operating conditions.

The distinction between the two methods becomes more pronounced when the load-torque disturbance is applied. As shown in Fig. 2(a), both controllers maintain speed tracking; however, the maximum speed deviation is $0.85983\,\mathrm{rad/s}$ for PID and only $0.23792\,\mathrm{rad/s}$ for SMC, corresponding to a reduction of approximately 72.3%. The tracking-error response in Fig. 2(b) further shows that SMC confines the error to a smaller magnitude and returns the system to the tracking condition more rapidly after the disturbance.

The post-disturbance integral indices further confirm this improvement. The IAE values of PID and SMC are 0.51395 and 0.03819, respectively, while the corresponding ITAE values are 0.23198 and 0.00508. Therefore, SMC reduces the IAE by approximately 92.6% and the ITAE by 97.8% relative to PID, indicating improved suppression of both error magnitude and error duration under load disturbance.

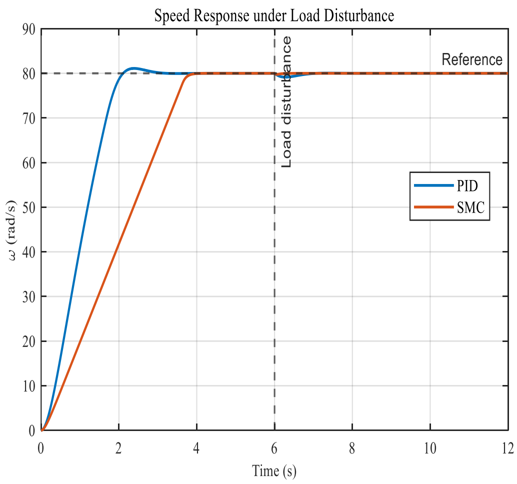

(a)

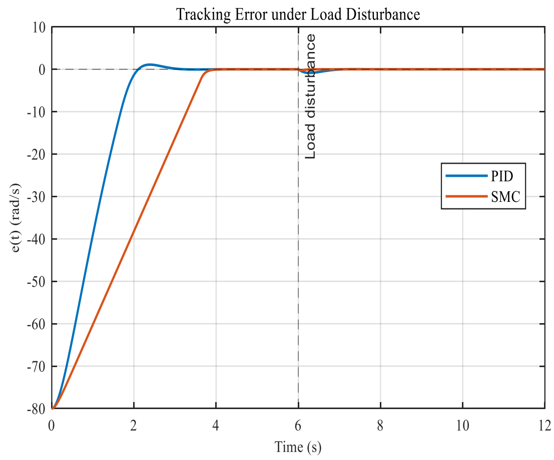

(b)

Fig. 2. System responses under load-torque disturbance: (a) rotor speed; (b) speed-tracking error.

The internal behavior of the SMC scheme is illustrated in Fig. 3. The sliding variable $s(t)$ converges to a neighborhood of zero after the reaching phase and remains within the boundary layer determined by $\phi = 3$. When the load disturbance is introduced at $t = 6$ s, the sliding variable is displaced only briefly before rapidly returning to the vicinity of the sliding manifold, which is consistent with the stability analysis in Section 3.
The control signal in Fig. 3(b) shows that SMC produces a strong corrective action when the disturbance is applied to compensate for the additional load torque and subsequently returns to a new steady-state level. Throughout the simulation, the control voltage satisfies the constraint ± 24 V, indicating that the required tracking performance is achieved without violating the actuator limitation.

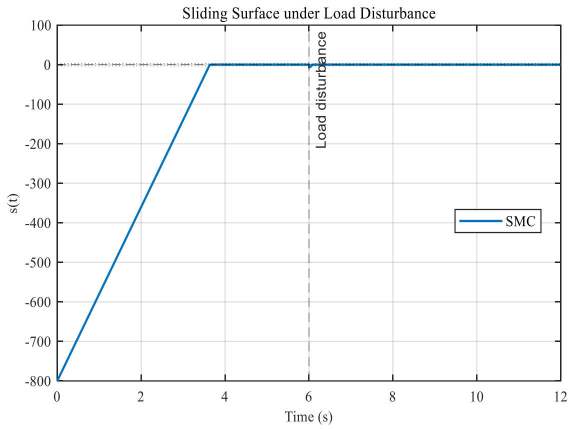

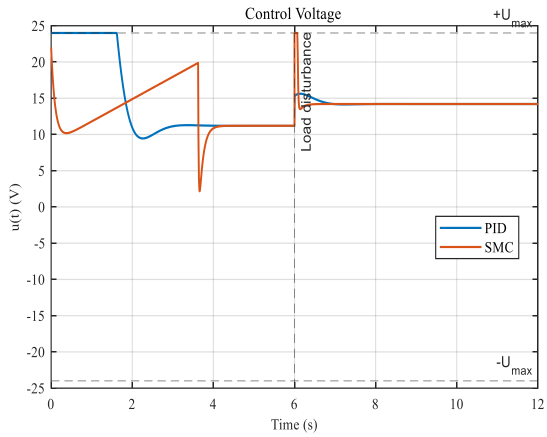

(a) **(b)**

Fig. 3. SMC characteristics under load disturbance: (a) sliding variable s(t); (b) control voltage.

Robustness is further examined by increasing the armature resistance, rotor inertia, and viscous friction coefficient by 30%, 50%, and 40%, respectively, while the load disturbance is still applied at $t = 6$ s. As shown in Fig. 4, both controllers preserve closed-loop stability and reference tracking without retuning. Nevertheless, SMC continues to exhibit a small speed deviation and favorable recovery behavior under the combined effects of model uncertainty and load disturbance, demonstrating robustness within the investigated uncertainty range.

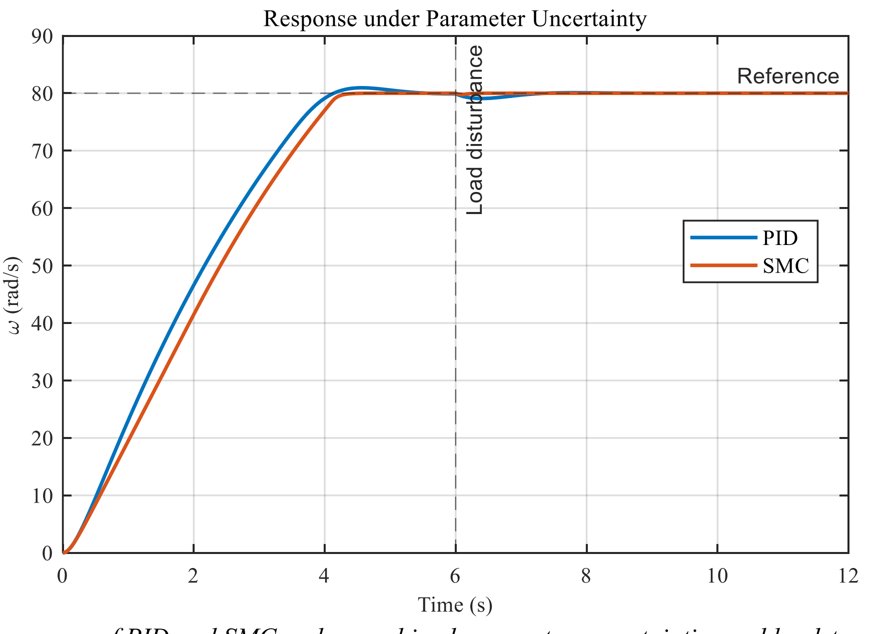

Fig. 4. Speed responses of PID and SMC under combined parameter uncertainties and load-torque disturbance.

The quantitative comparison is summarized in Table I. PID provides faster nominal transient performance, whereas SMC exhibits lower overshoot and markedly better load-disturbance rejection. In particular, the substantially lower IAE and ITAE values indicate that the principal advantage of SMC lies in preserving tracking quality in the presence of external disturbances and model mismatch.

TABLE I. QUANTITATIVE COMPARISON BETWEEN PID AND SMC CONTROLLERS

Performance metric	PID	SMC	SMC improvement
Maximum speed deviation $\Delta\omega max$ (rad/s)	0.85983	0.23792	72.3%
IAE after disturbance	0.51395	0.03819	92.6%
ITAE after disturbance	0.23198	0.00508	97.8%
Overshoot M_p (%)	1.3732	0	Eliminated

Note: The improvement is calculated as $(PID - SMC)PID.100\%$

Discussion: The PID controller provides a faster transient response under nominal operating conditions, as indicated by its shorter rise and settling times. However, the SMC scheme eliminates overshoot and exhibits significantly better load-disturbance rejection. Under the applied load-torque disturbance, SMC reduces the maximum speed deviation by approximately 72.3%, the IAE by 92.6%, and the ITAE by 97.8% compared with PID. These results indicate that the principal advantage of SMC does not lie in nominal startup speed, but rather in its ability to preserve tracking performance, limit error growth, and improve robustness in the presence of disturbances and parameter uncertainties.

V. CONCLUSION

This paper has presented the design and analysis of a Sliding Mode Control (SMC) scheme for speed regulation of a DC motor subject to load-torque disturbances and parameter uncertainties. The controller is derived from the electromechanical motor model, with convergence established through Lyapunov stability analysis. A saturation function is employed to mitigate chattering and improve compatibility with practical actuator constraints.

The results demonstrate that SMC preserves speed-tracking performance and closed-loop stability under varying operating conditions, whereas PID provides a faster transient response under nominal operation. These findings show that SMC is particularly attractive for DC motor drive applications requiring enhanced disturbance rejection and robustness to model uncertainty.

Within the scope of this study, the proposed method has been validated through numerical simulations over a predefined range of parameter variations. Future work will focus on further chattering reduction using higher-order sliding-mode techniques, systematic controller-parameter optimization, and experimental validation on a practical DC motor drive platform.

REFERENCES

[1] R. Krishnan, Electric Motor Drives: Modeling, Analysis, and Control. Upper Saddle River, NJ, USA: Prentice Hall, 2001.
[2] K. Ogata, Modern Control Engineering, 5th ed. Upper Saddle River, NJ, USA: Prentice Hall, 2010.
[3] G. F. Franklin, J. D. Powell, and A. Emami-Naeini, Feedback Control of Dynamic Systems, 8th ed. Hoboken, NJ, USA: Pearson, 2019.
[4] I. S. Okoro and C. O. Enwerem, “Robust control of a DC motor,” Heliyon, vol. 6, no. 12, Art. no. e05777, Dec. 2020, doi: 10.1016/j.heliyon.2020.e05777.
[5] A. T. Alexandridis and G. C. Konstantopoulos, “Modified PI speed controllers for series-excited DC motors fed by DC/DC boost converters,” Control Eng. Pract., vol. 23, pp. 14–21, Feb. 2014, doi: 10.1016/j.conengprac.2013.10.009.
[6] B. Hekimoğlu, “Optimal tuning of fractional order PID controller for DC motor speed control via chaotic atom search optimization algorithm,” IEEE Access, vol. 7, pp. 38100–38114, 2019, doi: 10.1109/ACCESS.2019.2905961.
[7] V. I. Utkin, “Variable structure systems with sliding modes,” IEEE Trans. Autom. Control, vol. 22, no. 2, pp. 212–222, Apr. 1977, doi: 10.1109/TAC.1977.1101446.
[8] J.-J. E. Slotine and S. S. Sastry, “Tracking control of nonlinear systems using sliding surfaces, with application to robot manipulators,” Int. J. Control, vol. 38, no. 2, pp. 465–492, 1983, doi: 10.1080/00207178308933088.
[9] K. D. Young, V. I. Utkin, and U. Özgüner, “A control engineer’s guide to sliding mode control,” IEEE Trans. Control Syst. Technol., vol. 7, no. 3, pp. 328–342, May 1999, doi: 10.1109/87.761053.
[10] V. Utkin, J. Guldner, and J. Shi, Sliding Mode Control in Electro-Mechanical Systems, 2nd ed. Boca Raton, FL, USA: CRC Press, 2009.
[11] A. Levant, “Higher-order sliding modes, differentiation and output-feedback control,” Int. J. Control, vol. 76, nos. 9–10, pp. 924–941, 2003, doi: 10.1080/0020717031000099029.
[12] A. Rauf, S. Li, R. Madonski, and J. Yang, “Continuous dynamic sliding mode control of converter-fed DC motor system with high order mismatched disturbance compensation,” Trans. Inst. Meas. Control, vol. 42, no. 14, pp. 2812–2821, Oct. 2020, doi: 10.1177/0142331220933415.
[13] N. Zhou, W. Deng, X. Yang, and J. Yao, “Continuous adaptive integral recursive terminal sliding mode control for DC motors,” Int. J. Control, vol. 96, no. 9, pp. 2190–2200, 2023, doi: 10.1080/00207179.2022.2086928.
[14] A. Ma’arif and A. Çakan, “Simulation and Arduino hardware implementation of DC motor control using sliding mode controller,” J. Robot. Control, vol. 2, no. 6, pp. 582–587, Nov. 2021, doi: 10.18196/jrc.26140.